

Synthesis, spectral studies, crystal structures and TDDFT studies of the rhenium(I) complexes of 2,4-dihydroxy-*N'*-(4-hydroxybenzilidene) benzohydrazide

Marta Sánchez-Lozano^a, Ezequiel M. Vázquez-López^{b,*}, José M. Hermida-Ramón^a, Carlos M. Estévez^a

^aDepartamento de Química Física, Facultad de Química, Universidade de Vigo, E-36310 Vigo, Galicia, Spain

^bDepartamento de Química Inorgánica, Facultad de Química, Universidade de Vigo, E-36310 Vigo, Galicia, Spain

ARTICLE INFO

Article history:

Received 20 November 2010

Accepted 23 December 2010

Available online 6 January 2011

Keywords:

Rhenium complexes

Carbonyl complexes

Schiff bases

DFT calculations

X-ray structures

ABSTRACT

The rhenium(I) carbonyl bromide complex, [ReBr(CO)₃(HL)], of the ligand derived from 2,4-dihydroxybenzaldehyde and 4-hydroxybenzoic acid hydrazide (HL), has been prepared. HL and its complex have been characterized by elemental analysis, MS, IR, UV–Vis and ¹H NMR spectroscopic methods. The structure of HL and the aqua-complex [Re(OH₂)(CO)₃(L)] where the ligands are monodeprotonated have been elucidated by X-ray diffraction. The structure of [ReBr(CO)₃(HL)] has been calculated from conformational parameters found in the aqua-complex. DFT and TDDFT calculations have been performed to obtain the IR spectra and UV–Vis absorption and emission spectra. The calculated spectra agree with the experimental results.

© 2011 Elsevier Ltd. All rights reserved.

1. Introduction

Rhenium(I) complexes containing fragments *fac*-[Re(CO)₃]⁺ have recently aroused attention because of the advantage of conjugating this fragment for labeling of targeting biomolecules.

Information obtained with the rhenium complex may be used as a hypothesis in the design of the analogs ^{99m}Tc to explore its application in nuclear medicine. Furthermore, the luminescent properties of rhenium(I) tricarbonyl complexes [1] have been demonstrated to have applications in biological imaging as fluorochromes in fluorescence microscopy [1,2]. The large Stokes shifts, long life times and good quantum yields allow easy differentiation of their emission from interfering autofluorescence [2].

A great deal of this work has focused on hydrazone derivatives containing N-heterocycles because of the high stability of {M(CO)₃}⁺ (M = Re, Tc) complexes, particularly pyridine, and their antitumor and antiviral activities [3]. Less interest has been received by acyl-hydrazone derivatives designed to O,N-coordination, in spite of preliminary results that suggest a closer affinity of rhenium(I) for N,O-chelate than N,N'-chelate [4].

Comparable stability may permit the formation of several complexes in the reaction medium used to prepare the radiopharm. From this point of view, linkage isomerism is a not desirable phenomenon in radiopharmaceuticals based on ^{99m}Tc because it may

result in a biodistribution of unpredictable characteristics. Furthermore, differentiation of multiple coordination modes in samples of Re^I/Tc^I complexes may be not possible by HPLC routine analysis [5,6]. Thus, spectroscopic tools may be suitable for coordinative diagnosis and detection of the isomers.

In the present paper, we report the study of a hydrazone derived from 2,4-dihydroxybenzoic and 4-hydroxycarbaldehyde (Scheme 1). The resulting hydrazone maintains structural relationship with diethylstilbestrol [7] and genistein [8] which are antagonists of the estrogen receptor (ER) α and β , respectively (Scheme 1). The two divergent –OH phenol groups are a pattern which is present in other ER targeting molecules such as raloxifene [9], while the acyl-hydrazone group may be used to anchor the metal to obtain radioimager of this receptor. Both the chelate ring and that formed by the intramolecular hydrogen bond (see HL in Scheme 1) should contribute to achieving the quasi planar conformation of estradiol.

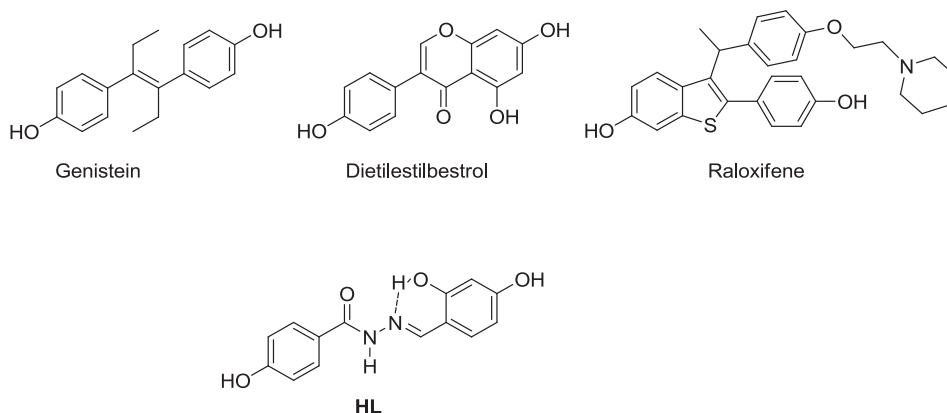
2. Results and discussion

2.1. Synthesis and spectroscopic characterization

The ligand HL was synthesized by Schiff base condensation using 4-hydroxybenzohydrazide and 2,4-dihydroxybenzaldehyde. Although the reaction of this ligand with *fac*-[ReX(CO)₃(CH₃CN)₂] (X = Cl, Br) were tried, only the bromide derivative was isolated as a solid. The last complex was isolated as an air stable solid

* Corresponding author.

E-mail address: ezequiel@uvigo.es (E.M. Vázquez-López).



Scheme 1.

moderately soluble in alcohols and other organic solvents, although with a lower solubility in chloroform. Elemental analysis and mass spectrometry (FAB) allow the establishment of the 1:1 stoichiometry. The mass spectrum contains signals with different intensity being the heaviest peak that corresponds to the $[M-Br]^+$. This specie is also observed in the spectra of all hydrazone complexes as the metallated peak with highest intensity. *Fac*- geometry around the rhenium atom is suggested by the three strong $\nu(\text{CO})$ IR bands in the range $2030\text{--}1900\text{ cm}^{-1}$. The group of bands in the range $1650\text{--}1600\text{ cm}^{-1}$, assigned to the carbonyl hydrazone group, is shifted to lower energy with the formation of the complex, which suggest that the hydrazone oxygen atom is involved in the coordination of the metal, as observed in the rhenium(I) complexes of the ferrocenyl carbaldehyde derivatives of 2-hydroxybenzoic acid hydrazide [10]. These bands are hardly modified when the carbonyl group is not involved in the coordination [11].

The ^1H NMR spectra of the rhenium(I) complex and ligand in acetone- d_6 were acquired and the assignments (see Fig. 1 for atom numbering scheme) are included in Section 3 for comparison.

The ^{15}N -HSQC experiments on HL and its complex allowed the assignment of the N-H signal. The O(3)-H proton is the most deshielded in the spectrum of HL and the next signal, at 10.94 ppm, is due to the N-H group. It was observed that, in general, the C-H proton signals in the rhenium complexes are shifted downfield with respect to those in the free ligand in hydrazone [10–12] and thiosemicarbazone [13–17] derivatives. In contrast, the hydrazone proton singlet is strongly shifted (about 2 ppm) when the N-H group is a member of the chelate ring [10,13] or by around 1 ppm when the N-H group does not form part of the ring [10,16]. The ^1H NMR spectrum of the complex shows substantial deshielding of the proton signals apart from the N-H group. On coordination, the N(1)-H proton gives rise to the most deshielded signal in the spectrum and the signal is shifted by 1.7 ppm with respect to that in the free ligand in agreement with the N,O-coordination of the ligand.

Furthermore, the rhenium(I) coordination breaks the intramolecular hydrogen bond O(3)-H...N(2) and, consequently, the magnetic behavior of this proton should be similar to the other O-H groups of the ligand. Thus, the three signals in the 9.5–9.3 ppm range are assigned to the corresponding O-H groups. Computational studies and the nature of the complex $[\text{Re}(\text{OH}_2)(\text{CO})_3(\text{L})]$, as revealed by X-ray diffraction (*vide infra*), suggest that the O(3)-H group establishes an intramolecular interaction as acceptor with the N(1)-H group. Consequently, a change of the configuration around the C(8)=N(1) is required: i.e. the *Z* configuration of the free ligand has to change to *E* (Scheme 2).

2.2. X-ray studies

2.2.1. The molecular structure of the compounds

The molecular structures and the numbering scheme of the free ligand and the rhenium(I) complex included in the present paper are shown in Fig. 1. Selected bond distances and angles are included in Table 1. Details about the data collection and refinements are included in Section 3.

The two aromatic rings in the structure of HL are almost coplanar. The configuration of the bonds involved in the hydrazone group are probably dominated by the hydrogen bonding between the O(3)-H group and N(2) atom. This interaction forms a six-membered ring that is also coplanar with the molecule plane and fixes the *E* configuration of the C(1)=N(1) bond. As in other acylhydrazone derived from aldehydes, the configuration of the bonds in the fragment C(1)-N(1)-N(2)-C(8) is *Z*, *E*, and *E*, respectively. The C-N and N-N distances in this fragment suggest mainly a double-bond character for the C(8)-N(2) link although some π -delocalization along the hydrazone chain is also possible.

Attempts to obtain single crystals of $[\text{ReBr}(\text{CO})_3(\text{HL})]$ were unsuccessful, but we have obtained single crystals of the deprotonated compound $[\text{Re}(\text{OH}_2)(\text{CO})_3(\text{L})]$. The formation of the rhenium(I) aqua complex by recrystallization of the halide complex is not without precedent. In fact, the formation of the aqua-complexes from the hydrazone precursor has been reported before [4,10]. This compound crystallized as a monohydrate compound $[\text{Re}(\text{OH}_2)(\text{CO})_3(\text{L})]\cdot\text{H}_2\text{O}$.

The rhenium atom is coordinated to N(2) and O(1) hydrazone atoms, by three carbon carbonyl atoms and by the oxygen of a water molecule. The resulting coordination geometry may be described as distorted octahedral, the main distortion being the N(2)-Re-O(1) angle. The Re-O(1) and Re-N(2) distances are very close to those found in the ferrocenylcarbaldehyde hydrazone complexes where we have observed O,N-coordination mode [10,12], in spite of the deprotonated nature of the hydrazone ligand in the last complexes. The poor sensitivity of the Re-L distances to the deprotonated nature of the ligand have been also observed in the rhenium(I) thiosemicarbazone complexes [13–15]. The distance Re(1)-O(1 W) is similar to those found in other hydrazone complexes [4,10], as well as phosphinite and phosphonite complexes [18].

Comparison of the distances in the hydrazone chain between the free ligand and the complex is difficult due to the high values of the esd's usually associated with the rhenium X-ray structures. Thus, the differences in the values of the distances N(1)-C(1) and N(8)-C(8) are statistically insignificant and they are not conclusive in the distances C(1)-O(1).

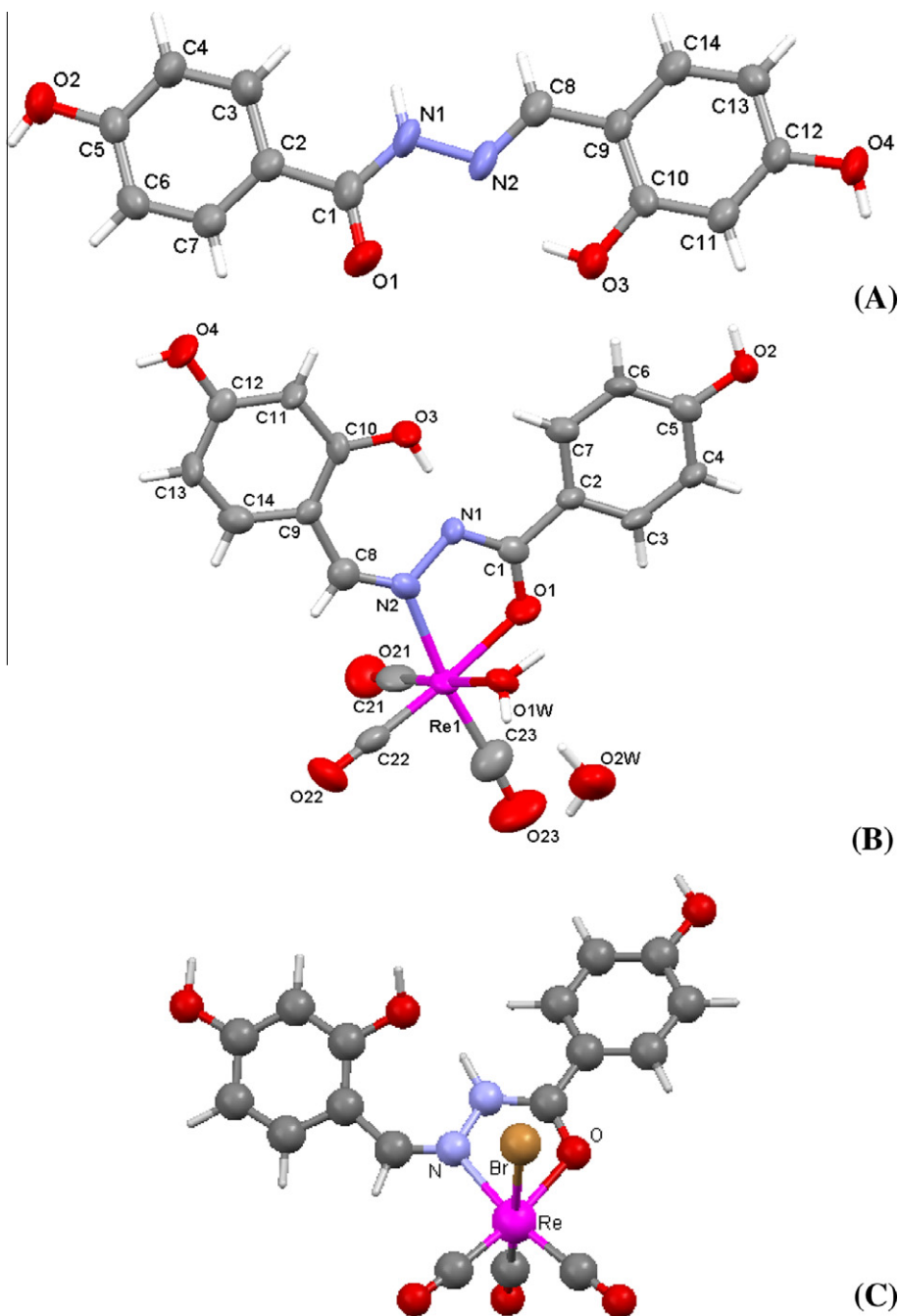
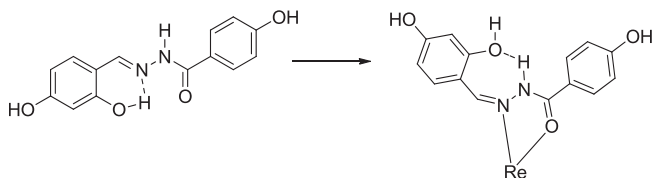


Fig. 1. X-ray (A and B) and computational (C) molecular structures of HL (A), $[\text{Re}(\text{OH}_2)(\text{CO})_3(\text{L})]$ (B) and $[\text{ReBr}(\text{CO})_3(\text{HL})]$ (C).



Scheme 2.

An interesting aspect of the structure is the effect on the configuration of the bond $\text{C}(8)=\text{N}(2)$ with the coordination. The $\text{O}(1), \text{N}(2)$ -coordination mode and the formation of the five-membered chelate ring of the ligand means the rupture of the intramolecular hydrogen bond $\text{O}(3)-\text{H} \cdots \text{N}(2)$. Now, the deprotonated $\text{N}(1)$

group may behave like an H-bonding acceptor, with the released $\text{O}(3)-\text{H}$ affording a new six-membered ring (Fig. 1B). The metric parameters associated with the $\text{O}(3)-\text{H} \cdots \text{N}(1)$ interaction are borderline between a strong and moderate hydrogen bond [19]. Note that this process supposes the change of the configuration around the $\text{C}(8)=\text{N}(2)$ bond from *E* to *Z*. We have observed the presence of both *Z*- and *E*-isomers in the rhenium(I) ferrocenyl thiosemicarbazones before [13], where both compounds were isolated as single crystals. In the present compound the intramolecular interaction is likely responsible for the stabilization of the isomer *Z*.

2.2.2. Crystal packing

The crystal packing in the structure of HL is strongly dominated by hydrogen bonding. The crystal structure may be described by

Table 1
Bond lengths (Å) and angles (°).

	HL		[ReBr(CO) ₃ (HL)]	[Re(OH ₂)(CO) ₃ (L)]·H ₂ O
	Experimental	Calculated	Calculated X = Br	Experimental X = O(1W)
Re(1)–C(21)			1.9080	1.840(15)
Re(1)–C(22)			1.9032	1.875(13)
Re(1)–C(23)			1.9249	1.885(15)
Re(1)–O(1)			2.1738	2.113(7)
Re(1)–N(2)			2.1978	2.148(8)
Re(1)–X			2.7082	2.161(8)
O(1)–C(1)	1.223(6)	1.2528	1.2795	1.267(11)
N(1)–C(1)	1.337(6)	1.3998	1.3719	1.355(12)
N(1)–N(2)	1.377(5)	1.3811	1.3994	1.410(10)
C(1)–C(2)	1.465(7)	1.4523	1.4724	1.488(13)
O(2)–C(5)	1.350(6)	1.3690	1.3903	1.357(11)
N(2)–C(8)	1.261(6)	1.3118	1.3135	1.292(12)
O(3)–C(10)	1.357(5)	1.3948	1.4112	1.320(11)
O(4)–C(12)	1.358(5)	1.3941	1.3870	1.364(11)
C(1)–N(1)–N(2)	119.7(5)	119.47	116.96	112.1(8)
O(1)–C(1)–N(1)	120.1(5)	121.84	119.09	122.5(10)
O(1)–C(1)–C(2)	121.9(5)	122.82	121.45	119.4(10)
N(1)–C(1)–C(2)	118.0(5)	115.33	119.45	118.0(9)
C(8)–N(2)–N(1)	117.7(5)	119.79	121.38	118.2(9)
N(2)–C(8)–C(9)	122.0(5)	120.26	134.74	132.9(11)
O(1)–Re(1)–N(2)			74.02	74.5(3)
O(1)–Re(1)–X			83.60	81.9(3)
N(2)–Re(1)–X			82.37	83.0(3)
C(1)–O(1)–Re(1)			116.80	115.9(7)

Table 2
Hydrogen bonds (Å and °).

D–H···A	d(D–H)	d(H···A)	d(D···A)	<(DHA)
<i>HL</i>				
O(3)–H(3)···N(2)	0.82	1.91	2.629(5)	145.0
O(2)–H(2)···O(4)#2	0.82	1.96	2.746(5)	160.3
N(1)–H(1)···O(3)#1	0.86	2.51	3.302(6)	152.9
O(4)–H(4)···O(1)#3	0.82	1.75	2.559(6)	169.5
Symmetry transformations used to generate equivalent atoms: #1 $x, -y + 1/2, z - 1/2$, #2 $x + 1, y + 1, z$, #3 $-x + 1, y - 1/2, -z + 1/2$.				
<i>[ReBr(CO)₃(HL)]^a</i>				
O(3)–H(3)···N(2)	1.0300	1.6700	2.6308	154.00
<i>[Re(OH₂)(CO)₃(L)]·H₂O</i>				
O(3)–H(3O)···N(1)	0.82	1.70	2.479(10)	157.7
O(2)–H(2O)···O(22)#1	0.82	2.26	3.005(11)	150.9
O(2)–H(2O)···O(21)#2	0.82	2.44	2.958(12)	121.6
O(4)–H(4O)···O(2)#3	0.82	2.15	2.888(11)	150.0
O(1W)–H(1W1)···O(3)#4	0.90(2)	1.85(6)	2.644(10)	146(10)
O(1W)–H(1W2)···O(2W)	0.90(2)	1.97(6)	2.736(12)	143(8)
O(2W)–H(2W1)···O(1)#5	0.999(12)	2.292(8)	3.202(15)	151.0(6)
O(2W)–H(2W2)···O(4)#6	0.906(10)	2.042(7)	2.898(12)	157.2(7)
Symmetry transformations used to generate equivalent atoms: #1 $x - 1, y + 1, z$; #2 $x, y + 1, z$; #3 $x, y - 1, z + 1$; #4 $-x + 1, -y + 1, -z + 1$; #5 $x + 1, y, z$; #6 $x + 1, y, z - 1$				

^a Calculated from the computational model.

taking into account the behavior of the three donor groups: two –OH and the hydrazone one, –N–H. The interaction O(2)–H···O(4)^{#2} (Table 2) arranges the molecules in chains (Fig. 2A). The interactions O(4)–H···O(1)^{#3} and N(1)–H···O(3)^{#1} cross equivalents chains produce the 3D net shown in Fig. 2B. The result is a rather effective packing and the Kitagoridskii index (KPI) is 72%.

The metallation and the presence of both water molecules (one of them coordinated) in [Re(OH₂)(CO)₃(L)]·H₂O modified substantially the molecular packing. The crystal structure may be described by considering the formation of the dimers (Fig. 3A) of the molecules by the interaction O(1W)–H···O(3)^{#4}. These dimers are now associated by the non-coordinated water molecule and by H-interactions involving the O–H groups in the net depicted in Fig. 3B. In this way, the packing in the structure of the complex (KPI = 71%) becomes as effective as the free ligand.

2.3. Computational studies

2.3.1. Geometries

The optimized geometry of the complex is shown in Table 1 and Fig. 1C along with the X-ray molecular structures. The structure of [ReBr(CO)₃(HL)] was calculated from the conformational parameters found in the aqua-complex. The calculated IR spectrum agrees with the experimental result for the complex (Fig. 4). On the other hand, the calculated bond distances and angles of the coordination sphere for the bromide complex are similar to those found in other N,O-acyl hydrazine complexes [4,10,12].

2.3.2. Orbital and UV–Vis spectra analysis

Before analyzing the absorption spectrum of the bromine complex it is a good idea to consider the main characteristics of the

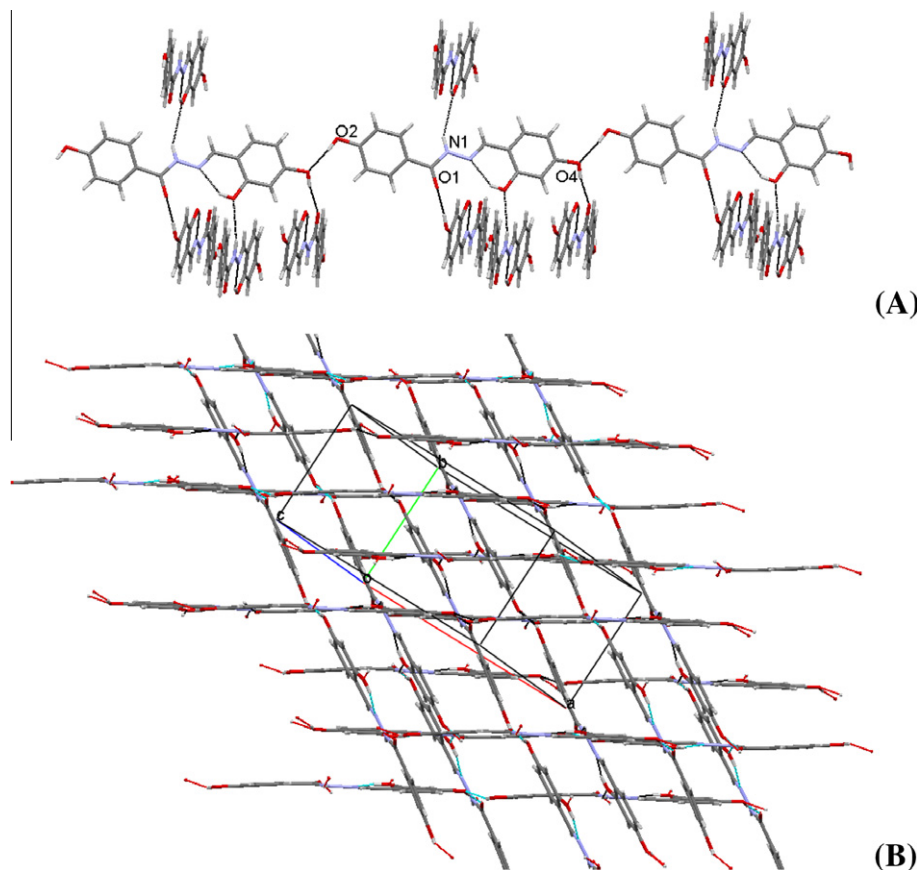


Fig. 2. Molecular packing in the X-ray structure of HL.

frontier molecular orbitals involved in the different transitions. The energy (in eV) and the composition in terms of contributions from the different groups to the MO of the 11 lowest virtual MOs and the 11 highest occupied MOs are shown in Table 3. Some of them are also drawn in Fig. 5.

The HOMO orbital of the complex is mainly composed by a π orbital of the ancillary ligand (40%) the d orbitals of the Re atom antibonding with the π orbital (27%) and a bromine orbital (19%). The LUMO orbital is roughly a π^* orbital of the ancillary ligand (93%). As can be seen in Fig. 5, the H-1 orbital comprise a d_{xy} orbital of Re (36%) antibonding with the orbital of bromine (40%). The H-2 can be described as a combination of a π orbital of the ligand (61%) and a bromine orbital (30%). The H-3 is basically a combination of a π orbital of the ligand (71%) and a bromine orbital (21%). H-4 is formed basically by a bonding combination of the d orbital of Re (63%) and the π^* orbital of the CO ligands.

Table 4 lists the 25 lower singlet excited states along with the corresponding wavelength of the transition from the ground state, the calculated oscillator strength, the major contributions to the final wavefunction, and the charge transfer after excitation for all 25 excited states.

Based on the calculated transitions, the band centered at 382 nm in the experimental spectrum (Fig. 4B) may originate from the transition $S_0 \rightarrow S_2$, with major contribution $H \rightarrow L$ (395 nm, $f=0.20$) and $S_0 \rightarrow S_3$ with major contribution $H-2 \rightarrow L$ (355 nm, $f=0.46$). Based on the frontier MO analysis and the excitation change transfer, this can be described as a MLCT, LLCT band. The transitions with the highest change transfer character ($S_0 \rightarrow S_1$ and $S_0 \rightarrow S_4$) have very small oscillator strengths and do not appear in the spectrum.

The second band centered at 304 nm is assigned to the $S_0 \rightarrow S_6$ transition, with major contribution $H-3 \rightarrow L$ (84%) (325 nm, $f=0.20$), and consequently may be characterized as a IL, LLCT band.

The third band centered at 255 nm can be tentatively assigned to a combination of different transitions, the most important are $S_0 \rightarrow S_{21}$ ($H-3 \rightarrow L+1$ (30%), $H-2 \rightarrow L+3$ (44%) (266 nm, $f=0.11$)) and $S_0 \rightarrow S_{22}$ ($H-2 \rightarrow L+2$ (29%), $H-2 \rightarrow L+3$ (-20%)). In both transitions the change transfer on excitation goes from the ligand and bromine atom to the CO ligands with little change on the Re atom.

The optimized structure for the S_1 excited state differs from the ground state mainly in the Re distances with the ligands and the C=O distances of the ancillary ligand and both N-C distances in the ancillary ligand. These changes in geometry are consequences of the change in electron density in the S_1 excited state, which is mainly a HOMO-LUMO transition and, as can be seen in Fig. 5, the change in electron density goes from the metal-ligand moiety to the ancillary ligand. The vertical difference in energy with the ground state is 2.575 eV, which gives a value of 481.5 nm for the emission wavelength in reasonable agreement with the experimental value of 460 nm (Fig. 4B).

In summary, in this work we have described the synthesis of a rhenium carbonyl bromide complex and a new N,O-acyl hydrazone ligand. X-ray studies show that the single crystals obtained from methanol solutions of this complex contain really the aqua complex and the deprotonated form of the ligand coordinated to rhenium atom. Furthermore, the configuration around of the azomethine C=N group (E) of the hydrazone ligand is different to that found in the X-ray structure of the free ligand (Z). DFT and TDDFT calculations, and spectroscopic studies of the bromide complex allow us to confirm the same configuration than in the aqua complex.

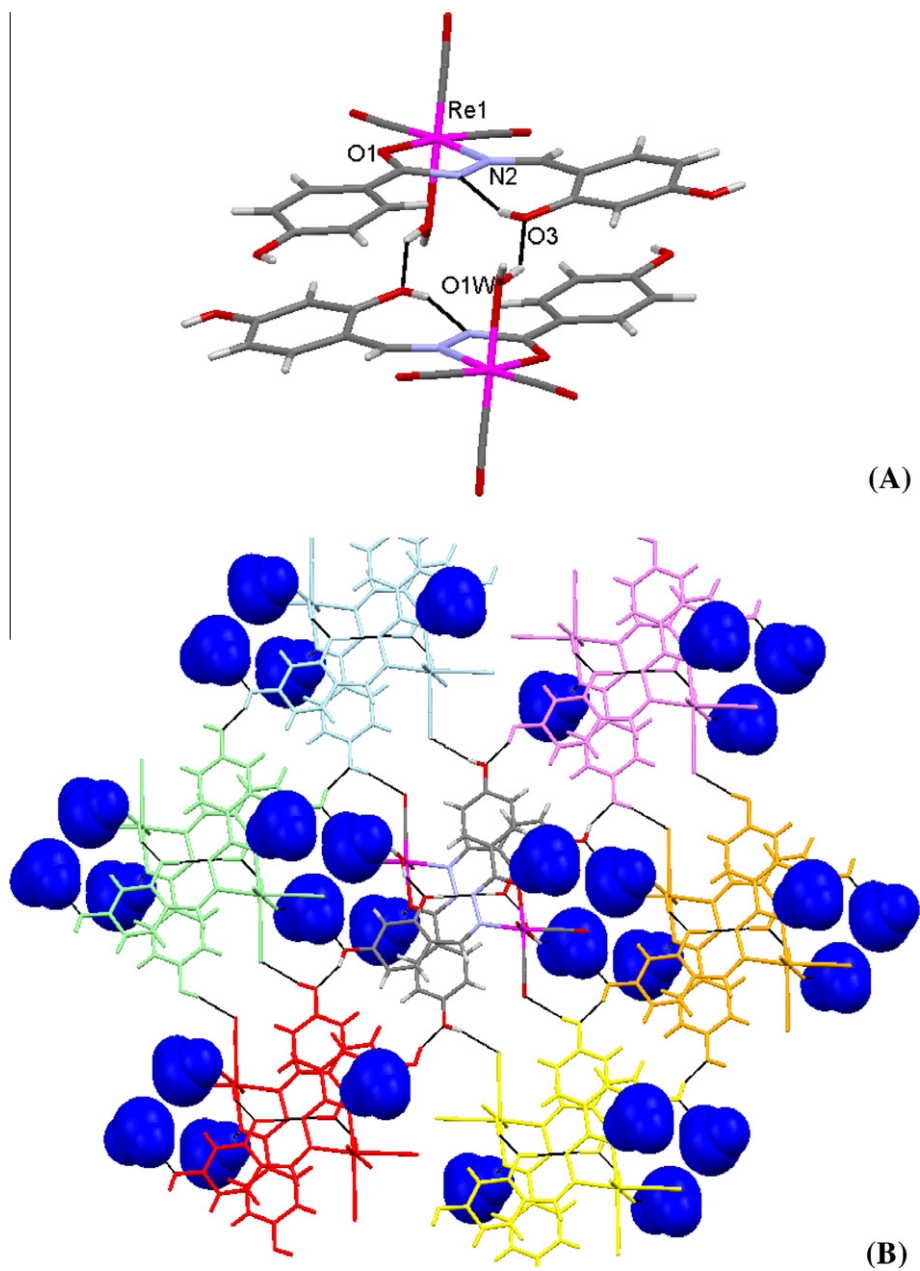


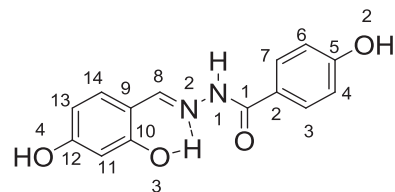
Fig. 3. Molecular packing in the X-ray structure of $[\text{Re}(\text{OH}_2)(\text{CO})_3(\text{L})]\cdot\text{H}_2\text{O}$.

3. Experimental

3.1. Materials and methods

All solvents were dried over appropriate drying agents, degassed using a vacuum line and distilled under an Ar atmosphere. $[\text{ReX}(\text{CO})_5]$ [20] and $[\text{ReX}(\text{CO})_3(\text{CH}_3\text{CN})_2]$ [21] were obtained by methods available in the literature.

Elemental analyses were carried out on a Fisons EA-1108. Melting points (m.p.) were determined on a Gallenkamp MFB-595 and are uncorrected. Mass spectra were recorded on a VG Autospec Micromass spectrometer operating under FAB conditions (nitrobenzyl alcohol matrix). Infrared spectra were recorded from KBr pellets on a Bruker Vector 22FT. UV–Vis (absorption and emission) spectra were obtained on HP 8453 and Horiba-Jobin-Yvon Fluoromax-3 TCSPC spectrophotometers. ^1H NMR spectra were obtained on a Bruker AMX 400 MHz spectrometer, from acetone- d_6 and DMSO- d_6 solutions, respectively.



3.2. X-ray data collection, structure determination and refinement

Crystallographic data collection and refinement parameters are listed in Table 5. All crystallographic measurements were performed on a Bruker Smart CCD apparatus at CACTI (University of Vigo) at r.t. (293(2) K) using graphite monochromated Mo $K\alpha$ radiation ($\lambda = 0.71073 \text{ \AA}$). The data were corrected for absorption effects using the program SADABS [22]. Structure analyses were carried out by direct methods [23]. Least-squares full-matrix

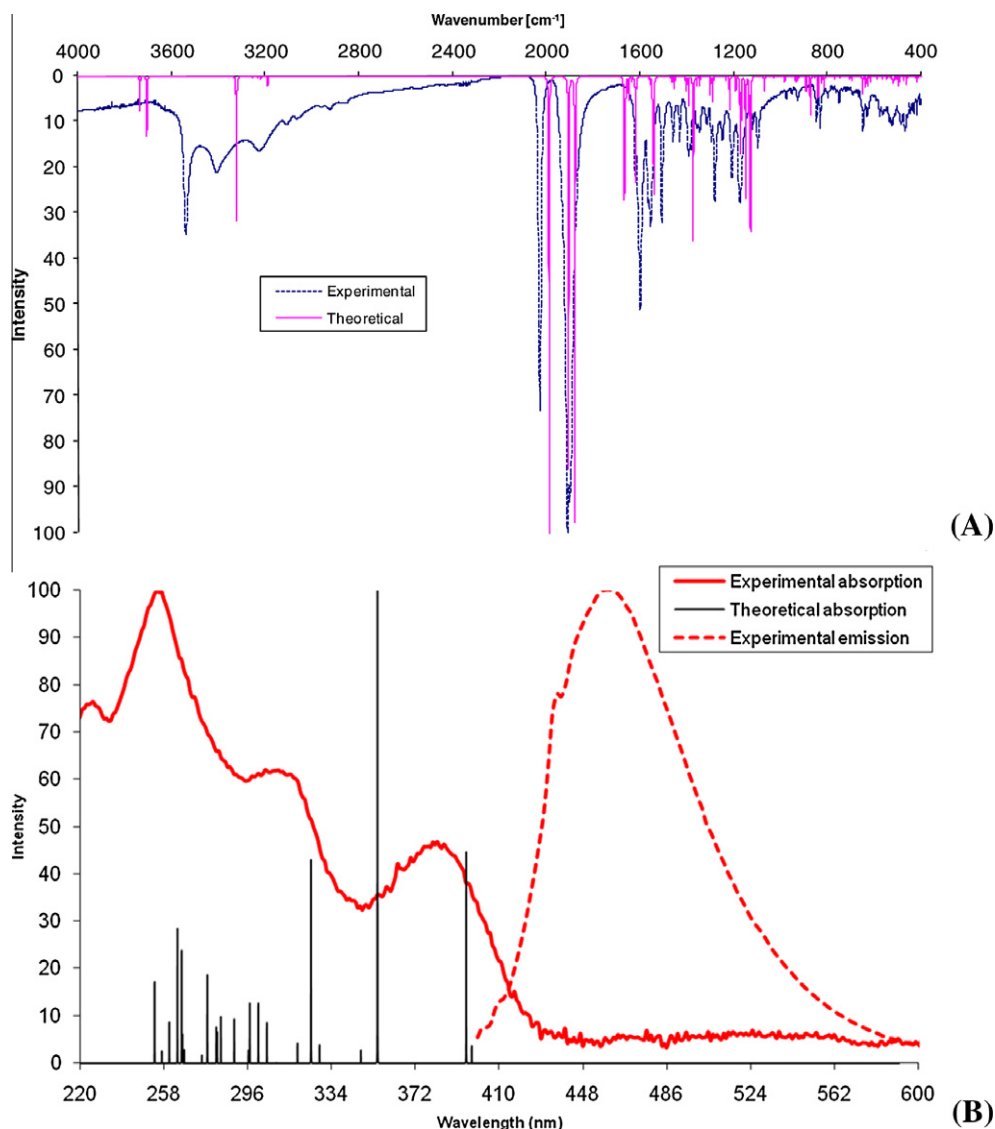


Fig. 4. Experimental and theoretical IR (A) and UV-Vis spectra (B) for $[\text{ReBr}(\text{CO})_3(\text{HL})]$.

refinements on F^2 were performed using the program *SHELXL97*. Atomic scattering factors and anomalous dispersion corrections for all atoms were taken from International Tables for Crystallography [24]. All non-hydrogen atoms were refined anisotropically. Hydrogen atoms were refined as riders. Graphics were obtained with *MERCURY* [25].

3.3. Computational details

Ground state geometries were optimized at the DFT level with the B3LYP functional. For the first row atoms we used the Dunning D95 V basis set [26a]. For Br and Re the Los Alamos ECP was employed [26b]. Neutral singlet ground state geometries were optimized at the DFT level with the B3LYP functional. Frequency calculations were performed on these structures. All their values were real, confirming that the structures are minima on the potential energy surface. Excitation energies and oscillator strengths were obtained by single point calculations on the optimized ground state geometries at the time dependent DFT (TDDFT) level for the lowest 25 singlet excited states. In order to emulate the solvent, a Polarized continuum model (PCM) [26c] where the solvent is simulated as a continuum with the dielectrical constant of meth-

Table 3
Energies and composition (%) of the MOs of the complex.

MO	eV	Contributions (%)			
		Re	CO	Br	Ligand
L+10	0.38	22	16	1	61
L+9	0.23	31	58	0	11
L+8	0.09	20	49	0	30
L+7	-0.12	40	54	2	4
L+6	-0.63	0	98	0	1
L+5	-0.81	0	0	0	100
L+4	-0.83	0	0	0	100
L+3	-1.36	20	70	5	5
L+2	-1.43	15	60	1	24
L+1	-1.71	8	17	1	74
LUMO	-2.61	2	4	2	93
HOMO	-6.33	27	13	19	40
H-1	-6.44	36	17	40	7
H-2	-6.64	6	3	30	61
H-3	-6.90	1	0	27	71
H-4	-6.96	63	31	0	6
H-5	-7.32	1	0	4	95
H-6	-7.49	24	10	38	27
H-7	-7.59	15	6	17	62
H-8	-7.60	14	6	15	64
H-9	-7.96	15	13	61	12
H-10	-8.45	9	3	16	71

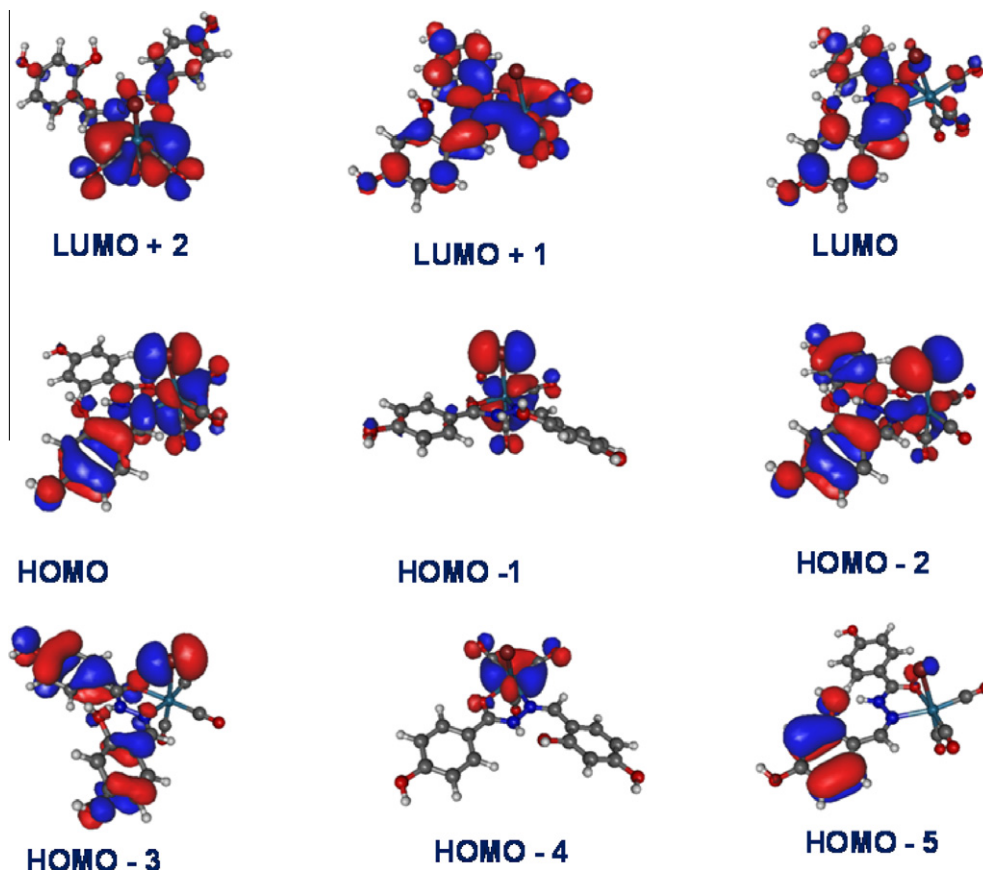


Fig. 5. Surface plot of the main frontier orbitals of $[\text{ReBr}(\text{CO})_3(\text{HL})]$.

Table 4
Excited states, wave lengths of the vertical excitation from the ground state, oscillator strengths, configurations with major contributions to the excited state, charge transfer after excitation (in a. u.), and assignment at the TDDFT B3LYP/LAN2DZ level in methanol for $[\text{ReBr}(\text{CO})_3(\text{HL})]$.

Excited state	λ (nm)		Osc. Strength	Major contributions	Charge transfer			
	Exp.	Calc.			Re	Br	ΣCO	HL
S_1	382	397.52	0.02	H - 1 \rightarrow LUMO (93%)	-33	-38	-13	85
S_2		395.01	0.20	H \rightarrow L (82%)	-24	-18	-9	52
S_3		354.72	0.46	H - 2 \rightarrow L (81%)	-6	-27	0	34
S_4		347.20	0.01	H - 4 \rightarrow L (96%)	-61	2	-27	87
S_5		328.44	0.02	H \rightarrow L + 1 (49%), H \rightarrow L + 2 (-35%)	-15	-19	24	11
S_6		324.56	0.20	H - 3 \rightarrow LUMO (84%)	0	-26	3	23
S_7	304	318.40	0.02	H - 1 \rightarrow L + 1 (47%), H - 1 \rightarrow L + 2 (-26%)	-22	-36	22	35
S_8		308.85	0.00	H - 1 \rightarrow L + 3 (77%)	-20	-32	48	4
S_9		304.52	0.04	H - 5 \rightarrow LUMO (83%)	-1	-4	5	0
S_{10}		300.62	0.06	H \rightarrow L + 1 (27%), H \rightarrow L + 2 (35%)	-15	-21	25	12
S_{11}		296.75	0.06	H - 1 \rightarrow L + 1 (32%), H - 1 \rightarrow L + 2 (20%), H \rightarrow L + 3 (-20%)	-18	-30	27	23
S_{12}		296.15	0.01	H - 7 \rightarrow L (14%), H - 6 \rightarrow L (66%)	-19	-31	-3	53
S_{13}		289.71	0.04	H - 1 \rightarrow L + 2 (30%), H \rightarrow L + 3 (31%)	-21	-23	47	-3
S_{14}		283.62	0.04	H - 7 \rightarrow L (42%), H - 2 \rightarrow L + 1 (-37%)	-7	-23	5	25
S_{15}		282.00	0.03	H - 8 \rightarrow L (58%), H - 7 \rightarrow L (19%)	-11	-17	0	28
S_{16}		281.52	0.03	H - 4 \rightarrow L + 1 (21%), H - 4 \rightarrow L + 3 (44%)	-42	-5	29	18
S_{17}		277.47	0.09	H - 8 \rightarrow L (-18%), H - 4 \rightarrow L + 3 (12%), H - 2 \rightarrow L + 1 (18%), H - 2 \rightarrow L + 2 (-15%)	-10	-20	18	12
S_{18}		275.01	0.01	H - 4 \rightarrow L + 1 (32%), H - 4 \rightarrow L + 3 (-24%)	-40	-4	23	23
S_{19}	255	266.99	0.01	H - 4 \rightarrow L + 1 (29%), H - 4 \rightarrow L + 2 (48%)	-47	-2	24	25
S_{20}		266.22	0.03	H - 3 \rightarrow L + 1 (38%), H - 2 \rightarrow L + 2 (-28%)	7	-30	37	-14
S_{21}		265.81	0.11	H - 3 \rightarrow L + 1 (30%), H - 2 \rightarrow L + 3 (44%)	7	-24	47	-30
S_{22}		263.90	0.13	H - 2 \rightarrow L + 2 (29%), H - 2 \rightarrow L + 3 (-20%)	7	-30	44	-21
S_{23}		260.21	0.04	H - 9 \rightarrow LUMO (75%)	-11	-58	-4	71
S_{24}		256.84	0.01	H \rightarrow L + 6 (40%)	-38	-17	76	-22
S_{25}		253.53	0.08	H - 5 \rightarrow L + 1 (-25%), H - 3 \rightarrow L + 2 (-20%), H \rightarrow L + 4 (27%)	-4	-16	18	2

anol was used. To estimate the emission bands, a TDDFT geometry optimization was done on the first single excited state of the Re

complex. This procedure has shown good performance for Re compounds [27–29]. All computations were done with the GAUSSIAN09

Table 5
Crystal data and structure refinement.

Identification code	HL	[Re(OH ₂)(CO) ₃ (L)]·H ₂ O
Empirical formula	C ₁₄ H ₁₂ N ₂ O ₄	C ₁₇ H ₁₅ N ₂ O ₉ Re
Formula weight	272.26	577.51
Crystal system	monoclinic	triclinic
Space group	P2(1)/c	P $\bar{1}$
Unit cell dimensions		
<i>a</i> (Å)	13.743(11)	6.9074(11)
<i>b</i> (Å)	7.872(6)	12.125(2)
<i>c</i> (Å)	11.976(10)	12.379(2)
α (°)	90	68.090(3)
β (°)	111.432(14)	77.999(4)
γ (°)	90	80.760(3)
<i>V</i> (Å ³)	1206.0(17)	936.9(3)
<i>Z</i>	4	2
<i>D_c</i> (Mg/m ³)	1.500	2.047
μ (mm ⁻¹)	0.112	6.540
θ Range (°)	1.59–25.06	1.80–25.06
<i>h k l</i> Ranges	–16, 14; –9, 9; –14, 12	–7, 8; –14, 14; –14, 14
Reflections collected	5877	5052
Independent reflections (<i>R_{int}</i>)	2115 (0.1177)	3271 (0.0580)
Goodness-of-fit on <i>F</i> ²	0.978	0.937
<i>R</i> ₁ and <i>wR</i> ₂ indices [<i>I</i> > 2 σ (<i>I</i>)]	0.0723, 0.1719	0.0502, 0.0748
<i>R</i> ₁ and <i>wR</i> ₂ indices (all data)	0.1870, 0.2359	0.1032, 0.0929

program package. [30] Analysis of the MOs and the excited state populations were performed with the GAUSSSUM program [31].

3.4. Synthesis of 2,4-dihydroxy-*N'*-(4-hydroxybenzylidene) benzohydrazide (HL)

A solution containing the 4-hydroxybenzohydrazide (442 mg, 2.90 mmol) with a stoichiometric amount of the 2,4-dihydroxybenzaldehyde (424 mg, 3.07 mmol) in ethanol (30 mL) was heated under reflux for 3 h and a small amount of acid was added. The pallid yellow solid formed was filtered off and vacuum dried over CaCl₂. Single crystals of ligand were obtained from a methanol solution after several days at room temperature. Yield: 621 mg (78%). M.p.: >260 °C. *Anal. Calc.* for C₁₄H₁₂N₂O₄ (272.26): C, 61.8; H, 4.4; N, 10.3. Found: C, 61.8; H, 4.5; N, 10.3%. Mass spectrum [*m/z* (%): 273.09 (100.00) [M+H]⁺. IR (KBr pellets, cm⁻¹): 3351s, 3110w, 3030w ν (OH) + ν (NH), 1633s, 1603s ν (C=O), 1545w, 1507s, 1454s ν (C=N) + ν (C=C).

¹H NMR (acetone-*d*₆, ppm): 11.85s (1) δ (O3–H), 10.94s (1) δ (N1–H), 8.84s (1), 9.02s (1) δ (O4,5–H), 7.87d (2) δ (C3,7–H), 6.94d (2) δ (C4,6–H), 8.45s (1) δ (C8–H), 7.16d (1) δ (C14–H), 6.43d (1) δ (C13–H), 6.41s (1) δ (C11–H). UV–Vis: λ in nm ($\epsilon \times 10^{-3}$; in L/mol cm), MeOH as solvent: absorption 265 (22.3), 316 (28.9), 363 (21.2). Emission ($\lambda_{\text{exc}} = 375$ nm) at 440 nm.

3.5. Synthesis of [ReBr(CO)₃(HL)]

A mixture of HL (36 mg, 0.13 mmol) and [ReBr(CO)₃(CH₃CN)₂] (55 mg, 0.13 mmol) in dry methanol (10 mL) was heated under reflux for 4 h. The solvent was reduced to approximately 5 mL and then a small amount of chloroform was added. The solution was dried on a rotary evaporator. The ochre-color solid obtained was filtered and dried in a vacuum. Yield: 42 mg (53%). M.p.: 210 °C. *Anal. Calc.* for C₁₇H₁₂N₂O₇BrRe (622.40): C, 32.8; H, 1.9; N, 4.5. Found: C, 32.0; H, 1.7; N, 4.5%. Mass spectrum [*m/z* (%): 543.02 (100.00) [M–Br]⁺. IR (KBr pellets, cm⁻¹): 3540s, 3409w, 3226w

ν (OH) + ν (NH), 2028vs, 1911vs, 1902vs ν (C=O), 1601s ν (C=O), 1558m, 1508m, 1460w, 1432w ν (C=N) + ν (C=C).

¹H NMR (acetone-*d*₆, ppm): 12.69s (1) δ (N1–H), 9.54s (1), 9.53 (1) δ (O4,5–H), 9.32s (1) δ (O3–H), 8.06d (2) δ (C3,7–H), 7.05d (2) δ (C4,6–H), 9.04s (1) δ (C8–H), 8.30d (1) δ (C14–H), 6.61d (1) δ (C13–H), 6.53s (1) δ (C11–H). UV–Vis: λ in nm ($\epsilon \times 10^{-3}$; in L/mol cm), MeOH as solvent: absorption 255 (21.3), 304 (13.2), 382 (10.0). Emission ($\lambda_{\text{exc}} = 385$ nm) at 460 nm.

3.6. Formation of [Re(OH₂)(CO)₃(L)]·H₂O

This compound was obtained as single crystals in a methanol solution after several days at r.t. The crystals isolated were too few for elemental analysis or meaningful estimation of yield.

Acknowledgements

Financial support from the ERDF (EU) and the MCI (Spain) (Research Project CTQ2010-19386/BQU) is gratefully acknowledged.

Appendix A. Supplementary data

CCDC 801248 and 801249 contain the supplementary crystallographic data for HL and ([Re(OH₂)(CO)₃(L)]). These data can be obtained free of charge via <http://www.ccdc.cam.ac.uk/conts/retrieving.html>, or from the Cambridge Crystallographic Data Centre, 12 Union Road, Cambridge CB2 1EZ, UK; fax: (+44) 1223-336-033; or e-mail: deposit@ccdc.cam.ac.uk.

References

- [1] A.J. Amoroso, M.P. Coogan, J.E. Dunne, V. Fernández-Moreira, J.B. Hess, A.J. Hayes, D. Lloyd, C. Millet, S.J.A. Pope, C. Williams, *Chem. Commun.* (2007) 3066–3068.
- [2] A.J. Amoroso, R.J. Arthur, M.P. Coogan, J.B. Court, V. Fernández-Moreira, A.J. Hayes, D. Lloyd, C. Millet, S.J.A. Pope, *New J. Chem.* 32 (2008) 1097.
- [3] M.A. Ali, R.N. Bose, *Polyhedron* 3 (1984) 517.
- [4] J. Grewe, A. Hagenbach, B. Stromburg, R. Alberto, E. Vázquez-López, U. Abram, *Z. Anorg. Allg. Chem.* 629 (2003) 303.
- [5] H. He, M. Lipowska, X. Xu, A.T. Taylor, M. Carlone, L.G. Marzilli, *Inorg. Chem.* 44 (2005) 5437.
- [6] H. He, J.E. Morley, B. Twamley, R.H. Groeneman, D. Bucar, L.R. MacGillivray, P.D. Benny, *Inorg. Chem.* 48 (2009) 10625.
- [7] A.K. Shiau, D. Barstad, P.M. Loria, L. Cheng, P.J. Kushner, D.A. Agard, G.L. Greene, *Cell* 95 (1998) 927.
- [8] E.S. Manas, Z.B. Xu, R.J. Unwalla, W.S. Somers, *Structure* 12 (2004) 2197.
- [9] A.M. Brzozowski, A.C.W. Pike, Z. Dauter, R.E. Hubbard, T. Bonn, O. Engstrom, L. Ohman, G.L. Greene, J. Gustafsson, M. Carlquist, *Nature* 389 (1997) 753.
- [10] P. Barbazán, R. Carballo, I. Prieto, M. Turnes, E.M. Vázquez-López, *J. Organomet. Chem.* 694 (2009) 3102.
- [11] P. Barbazán, A. Hagenbach, E. Oehlke, U. Abram, R. Carballo, S. Rodríguez-Hermida, E.M. Vázquez-López, *Eur. J. Inorg. Chem.* (2010) 4622–4630.
- [12] P. Barbazán, R. Carballo, U. Abram, G. Pereiras-Gabián, E.M. Vázquez-López, *Polyhedron* 25 (2006) 3343.
- [13] R. Carballo, J.S. Casas, E. García-Martínez, G. Pereiras-Gabián, A. Sánchez, J. Sordo, E.M. Vázquez-López, J.C. García-Monteaudo, U. Abram, *J. Organomet. Chem.* 656 (2002) 1.
- [14] A. Núñez-Montenegro, R. Carballo, E.M. Vázquez-López, *Polyhedron* 28 (2009) 3915.
- [15] A. Núñez-Montenegro, R. Carballo, E.M. Vázquez-López, *Polyhedron* 27 (2008) 2867.
- [16] R. Carballo, J.S. Casas, E. García-Martínez, G. Pereiras-Gabián, A. Sánchez, U. Abram, E.M. Vázquez-López, *CrystEngComm* 7 (2005) 113.
- [17] R. Carballo, J.S. Casas, E. García-Martínez, G. Pereiras-Gabián, A. Sánchez, J. Sordo, E.M. Vázquez-López, *Inorg. Chem.* 42 (2003) 6395.
- [18] R. Carballo, A. Castiñeiras, S. García-Fontán, P. Losada-González, U. Abram, E.M. Vázquez-López, *Polyhedron* 20 (2001) 2371.
- [19] G.A. Jeffrey, *An Introduction to Hydrogen Bonding*, Oxford University Press, New York, 1997.
- [20] S.P. Schmidt, W.C. Troglor, F. Basolo, *Inorg. Synth.* 28 (1990) 160.
- [21] M.F. Faron, K.F. Kraus, *Inorg. Chem.* 9 (1970) 1700.
- [22] G.M. Sheldrick, *SAINT v. 6.22*, Bruker AXS, 2001.
- [23] G.M. Sheldrick, *SHELX-97*, Program for the Solution and Refinement of Crystal Structures, v.2, 1997.
- [24] A.J.C. Wilson, *International Tables for Crystallography*, vol. C, Kluwer Academic Press, Dordrecht, The Netherlands, 1992.

- [25] I.J. Bruno, J.C. Cole, P.R. Edgington, et al., *Acta Crystallogr., Sect. B* 58 (2002) 389.
- [26] (a) T.H. Dunning Jr., P.J. Hay, in: H.F. Schaefer III. (Ed.), *Modern Theoretical Chemistry*, vol. 3, Plenum, New York, 1976, pp. 1–28;
(b) P.J. Hay, W.R. Wadt, *J. Chem. Phys.* 82 (1985) 270–283;
(c) V. Barone, M. Cossi, *J. Phys. Chem. A* 102 (1998) 1995–2001.
- [27] S. Basak, D. Chopra, K.K. Rajak, *J. Organomet. Chem.* 693 (2008) 2649.
- [28] B. Machura, M. Wolff, J. Kusz, *Polyhedron* 29 (2010) 1619.
- [29] X. Li, X. Liu, Z. Wu, H. Zhang, *J. Phys. Chem. A* 112 (2008) 11190.
- [30] M.J. Frisch, G.W. Trucks, H.B. Schlegel, G.E. Scuseria, M.A. Robb, J.R. Cheeseman, J.A. Jr. Montgomery, T. Vreven, K.N. Kudin, J.C. Burant, J.M. Millam, S.S. Iyengar, J. Tomasi, V. Barone, B. Mennucci, M. Cossi, G. Scalmani, N. Rega, G.A. Petersson, H. Nakatsuji, M. Hada, M. Ehara, K. Toyota, R. Fukuda, J. Hasegawa, M. Ishida, T. Nakajima, Y. Honda, O. Kitao, H. Nakai, M. Klene, X. Li, J.E. Knox, H.P. Hratchian, J.B. Cross, V. Bakken, C. Adamo, J. Jaramillo, R. Gomperts, R.E. Stratmann, O. Yazyev, A.J. Austin, R. Cammi, C. Pomelli, J.W. Ochterski, P.Y. Ayala, K. Morokuma, G.A. Voth, P. Salvador, J.J. Dannenberg, V.G. Zakrzewski, S. Dapprich, A.D. Daniels, M.C. Strain, O. Farkas, D.K. Malick, A.D. Rabuck, K. Raghavachari, J.B. Foresman, J.V. Ortiz, Q. Cui, A.G. Baboul, S. Clifford, J. Cioslowski, B.B. Stefanov, G. Liu, A. Liashenko, P. Piskorz, I. Komaromi, R.L. Martin, D.J. Fox, T. Keith, M.A. Al-Laham, C.Y. Peng, A. Nanayakkara, M. Challacombe, P.M.W. Gill, B. Johnson, W. Chen, M.W. Wong, C. Gonzalez, J.A. Pople, Gaussian 03, Gaussain Inc. Wallingford CT, 2004.
- [31] N.M. O'boyle, A.L. Tenderholt, K.M. Langner, *J. Comp. Chem.* 29 (2008) 839.